JOURNAL OF PROPULSION AND POWER
Vol. 22, No. 4, July–August 2006

Film-Cooling Effectiveness on Squealer Cavity and Rim Walls of Gas-Turbine Blade Tip

Shantanu Mhetras,* Huitao Yang,* Zhihong Gao,* and Je-Chin Han†
Texas A&M University, College Station, Texas 77843-3123

Effects of shaped holes on the tip pressure side, coolant jet impingement on the pressure side squealer rim from tip holes, and varying blowing ratios for a squealer blade tip were examined on film-cooling effectiveness. The film-cooling effectiveness distributions were measured on the blade tip, near tip pressure side, and the inner pressure side rim wall using pressure-sensitive-paint technique. Air and nitrogen gas were used as the film-cooling gases, and the oxygen concentration distribution for each case was measured. The film-cooling effectiveness information was obtained from the difference of the oxygen concentration between air and nitrogen gas cases by applying the mass-transfer analogy. The internal coolant-supply passages of the squealer tipped blade were modeled similar to those in the GE-E^3 rotor blade with two separate serpentine loops supplying coolant to the film-cooling holes. A row of compound angled cylindrical film-cooling holes was arranged along the camber line on the tip and another row of compound angled shaped film-cooling holes was arranged along the span of the pressure side just below the tip. The average blowing ratio of the cooling gas was controlled to be 0.5, 1.0, and 2.0. Tests were conducted in a five-bladed linear cascade in a blowdown facility with a tip gap clearance of 1.5%. The freestream Reynolds number, based on the axial chord length and the exit velocity, was 1.48×10^6, and the inlet and the exit Mach number were 0.23 and 0.65, respectively. Turbulence intensity level at the cascade inlet was 9.7%. Numerical predictions were also performed using Fluent to simulate the experiment at the same inlet flow conditions. Predictions for film cooling are presented. Results show a good correlation between experimental and predicted data. The shape and location of the film-cooling holes along with varying blowing ratios can have significant effects on film-cooling performance.

Nomenclature

C	=	tip clearance gap (1.5% span)
C_D	=	discharge coefficient
C_x	=	axial chord length of the blade (8.61 cm)
Co	=	oxygen concentration
d	=	diameter of film-cooling holes
I	=	pixel intensity for an image
M	=	average blowing ratio ($=\rho_c V_c/\rho_m V_{\text{avg}}$)
M_i	=	Local blowing ratio ($=\rho_{\text{c,local}} V_{\text{c,local}}/\rho_{\text{m,local}} V_{\text{m,local)}}$
P	=	local static pressure
P_{O_2}	=	partial pressure of oxygen
P_t	=	total pressure
T_c	=	temperature of coolant at loop inlet
Tu	=	turbulence intensity level at the cascade inlet
x	=	axial distance, cm
V_{avg}	=	averaged velocity of mainstream air at cascade inlet and exit
V_c	=	averaged velocity of coolant air from all film-cooling holes in each loop
y^+	=	dimensionless distance from wall
η	=	local film-cooling effectiveness
θ	=	dimensionless temperature $= (T_{\text{film}} - T_{\text{coolant}})/(T_{\text{mainstrm}} - T_{\text{coolant}})$
ρ_c	=	density of coolant air
ρ_m	=	density of mainstream air

Subscripts

air	=	mainstream air with air as coolant
blk	=	image without illumination (black)
mix	=	mainstream air with nitrogen as coolant
ref	=	reference image with no mainstream and coolant flow

Introduction

THE concept of cooling a surface subjected to high mainstream temperatures by perforating the surface with several discrete holes and passing cold air (film cooling) through them is a popular technique used in several applications. The surface under test can be maintained at a cooler temperature caused by formation of a thin protective film of relatively colder air on the surface. This technique has been successfully employed for cooling of gas-turbine blades subjected to very high mainstream gas temperatures. A high and uniform film-cooling effectiveness on the blade surface will ensure superior performance and thermal fatigue life for the blade, thus making it an important parameter in its design.

Hot gases from the combustor enter the turbine, resulting in a significant heat load on the turbine components. One of the components more susceptible to thermal failure is the blade-tip region because of its severe environment and difficulty in cooling. Large leakage flow occurs on the tip as a result of a high pressure differential from pressure to suction side. This leakage mass flow can be reduced by using a labyrinth-like recessed cavity also known as the squealer tip. Presence of film cooling on the tip further reduces heat transfer from the mainstream gas to the blade tip. A comprehensive compilation of the available cooling techniques used in the gas-turbine industry has been encapsulated by Han et al.[1]

Experimental investigations performed in the general area of film cooling on a blade tip are limited with few papers available in open literature. Film cooling on a blade tip was first studied by Kim and Metzger[2] and Kim et al.[3] by using a two-dimensional rectangular tip model to simulate leakage flow between the tip and the shroud. Various film-cooling configurations were examined using a transient liquid crystal technique, and the results for heat-transfer coefficients and film-cooling effectiveness were reported. Kwak and Han[4,5] studied the local heat-transfer distribution and film-cooling effectiveness

Received 29 July 2005; revision received 24 November 2005; accepted for publication 25 November 2005.

*Research Assistant, Department of Mechanical Engineering.
†M.C. Easterling Chair Professor, Turbine Heat Transfer Laboratory, Department of Mechanical Engineering. Associate Fellow AIAA.

using hue-detection-based transient liquid crystal technique on the blade tip for plane and squealer tip geometry. A GE-E^3, five-blade linear cascade was used similar to the one used in the present paper. They used three tip gap clearances (1.0, 1.5, and 2.5% of blade span) along with three average blowing ratios (0.5, 1.0, and 2.0) for the coolant. Increasing blowing ratio increased film effectiveness, but overall heat-transfer coefficients decreased. Their results also showed that the squealer geometry showed higher film-cooling effectiveness and lower heat-transfer coefficients compared to the plane tip geometry because of its smaller leakage flow.

Ahn et al.[6] presented film-cooling effectiveness results using the Pressure-Sensitive-Paint (PSP) technique on a plane and squealer blade tip with one row of holes on the camber line and another row of angled holes near the pressure-side tip. They used the same high flow cascade as the present study and investigated the effects of tip gap clearance (1.0, 1.5, and 2.5% blade span) and blowing ratio ($M = 0.5$, 1, and 2). They noted that higher blowing ratios give higher effectiveness. Results with plane tip showed clear traces of the coolant path, whereas for squealer tip, coolant accumulation effects were observed on the cavity floor. Christophel et al.[7,8] studied film cooling and heat transfer using the infrared technique on a plane tip under low-speed conditions. They used four different coolant flow rates (0.47, 0.58, 0.68, and 1.0% passage flow) for two tip gaps. A row of holes was located on the pressure side just below the tip with two more dirt purge holes on the tip itself. They found that a smaller tip gap and larger coolant flow showed better cooling. They also found that higher blowing ratios resulted in higher augmentations on tip heat transfer but with an overall net heat-flux reduction when combined with adiabatic effectiveness measurements.

Some experimental investigations have also been performed to study heat transfer on the blade tip under rotating conditions. Heat-transfer coefficients on the blade tip and the shroud were measured by Metzger et al.[9] using heat-flux sensors in a rotating turbine rig. Dunn and Haldeman[10] measured time-averaged heat flux at a recessed blade tip for a full-scale rotating turbine stage at transonic vane exit conditions. Their results showed that the heat-transfer coefficient at the mid and rear portion of the cavity floor is of the same order as the blade leading-edge value.

There are many papers available in open literature, which discuss heat-transfer coefficients on the blade-tip and near-tip regions. Several of these papers present results under engine representative mainstream flow conditions. Local heat-transfer coefficients on a turbine blade-tip model with a recessed cavity (squealer tip) were studied by Yang and Diller[11] in a stationary transonic linear cascade. Based on measurements at a single point on the cavity floor, they reported that heat-transfer coefficients were independent of the tip gap height. Bunker et al.[12] utilized a hue-detection based liquid crystal technique to obtain local heat-transfer distributions on a plane blade tip in a stationary cascade. They studied the effects of tip gap clearance and freestream turbulence intensity levels. Azad et al.[13,14] used transient liquid crystal technique to study heat transfer. They compared squealer-tip and plane-tip geometry and concluded that the overall heat-transfer coefficients were lower for squealer tip case. Bunker and Bailey[15] studied the effect of squealer cavity depth and oxidation on turbine blade-tip heat transfer. Azad et al.[16] and Kwak et al.[17] investigated the heat transfer on several different squealer geometries. They found that a suction-side squealer tip gave the lowest heat-transfer among all cases studied. Heat-transfer coefficient distributions for plane- and squealer-tip and near-tip regions were presented by Kwak and Han[18,19] in two papers. By using a squealer tip, heat transfer was found to decrease on the tip and near-tip regions.

A few of the many papers on blade-tip heat/mass transfer performed under low-speed conditions are also discussed. Investigations comparing a rotating and stationary shroud were performed by Mayle and Metzger.[20] They noted that the effect of shroud rotation could be neglected to measure the blade-tip heat transfer over the entire range of parameters considered in the study. Heyes et al.[21] studied tip leakage flow on plane and squealer tips in a linear cascade and concluded that the use of a squealer tip, especially a suction-side squealer tip, was more beneficial than a flat tip. Heat-transfer coefficients and static-pressure distributions of a large-scale turbine blade tip were measured by Teng et al.[22] in a low-speed wind tunnel facility using a transient liquid crystal technique. Mass-transfer technique was used by Papa et al.[23] to study local and average mass/heat-transfer distributions on a squealer tip and winglet-squealer tip in a low-speed wind tunnel. Jin and Goldstein[24,25] also used this technique on a simulated high-pressure turbine blade-tip and near-tip surfaces. They concluded that the average mass transfer from the tip surface was much higher than that on pressure-and suction-side surfaces. Saxena et al.[26] investigated the effect of various tip sealing geometries on blade-tip leakage flow and heat transfer of a scaled-up high pressure (HP) turbine blade in a low-speed wind-tunnel facility using a steady-state hue saturation intensity (HSI-) based liquid crystal technique. They noted that the trip strips placed against the leakage flow produce the lowest heat transfer on the tips compared to all of the other cases.

Some numerical investigations have also been carried out to study heat transfer and film-cooling effectiveness on blade tip. Effects of tip clearance and casing recess on heat transfer and stage efficiency for several squealer blade-tip geometries were predicted by Ameri et al.[27] Ameri and Rigby[28] also calculated heat-transfer coefficients and film-cooling effectiveness on turbine-blade models. Numerical results for heat transfer and flow obtained by Ameri et al.[29] were compared to the experimental results from Bunker et al.[12] for a power-generation gas turbine.

Numerical techniques were also utilized by Yang et al.[30,31] to study flow and heat transfer past a turbine blade with plane and squealer tip. Film-cooling effectiveness for a flat and squealer blade tip with film-cooling holes on tip pressure side were predicted by Acharya et al.[32] Hohlfeld et al.[33] predicted film-cooling flow from dirt purge holes on a turbine blade tip. They found that the flow exiting the dirt purge holes helped in blocking the leakage flow across the gap. As the blowing ratio increased for a large tip gap, tip cooling increased only slightly, whereas film cooling on the shroud increased significantly. Effects of different hole locations on film-cooling effectiveness and heat transfer were predicted by Yang et al.[34]

The main focus of the present study is to investigate the effects of film cooling on the squealer rim walls and the squealer cavity floor. The pressure-side rim wall is prone to high heat-transfer coefficients because of the large leakage flow, comparable to the leading edge of the blade. This can result in oxidation of the blade-tip rim as a result of high metal temperatures, as it is difficult to cool the entire blade tip uniformly. Rubbing of the tip with the shroud can cause further erosion of the squealer rim, thus increasing the tip gap and leakage flow, which will further increase the heat-transfer coefficients. Continued operation under these severe conditions can make the blade more susceptible to failure. By using film cooling, contact of the hot gases with the rim wall surface can be reduced, thus reducing the overall net heat flux into the blade. Currently, no data are available in open literature for film-cooling effectiveness on the pressure-side outer and inner rim walls. Heat-transfer data are also limited in this region mainly because of large experimental uncertainty because of heat-conduction errors in the thin rim wall.

A scaled-up blade-tip model of a first-stage rotor blade (GE-E^3) of a modern aircraft gas turbine was used in a five-blade linear cascade with the center blade tip coated with PSP. In this study, the presence of a row of nine-compound angled, shaped film-cooling holes on the near-tip pressure side and another row of eight compound angled cylindrical holes on the cavity floor were studied on film-cooling effectiveness. Serpentine passages similar to those for a GE-E^3 HP turbine rotor blade were modeled to supply coolant to these film-cooling holes. The hole location, shape, orientation, and internal coolant flowpath are different from Ahn et al.[6] and much closer to a real gas-turbine blade-tip design. Film-cooling effectiveness was studied on the rim, cavity floor, inner cavity walls, and the near-tip pressure side. Moreover, the PSP technique is based on mass-transfer analogy, which eliminates any heating/conduction errors present in other measurement techniques such as liquid crystal, infrared (IR) camera, or foil heater. Experiments were carried out to study pressure and effectiveness for squealer blade tip for a tip clearance of 1.5% of blade span with the average blowing ratios of

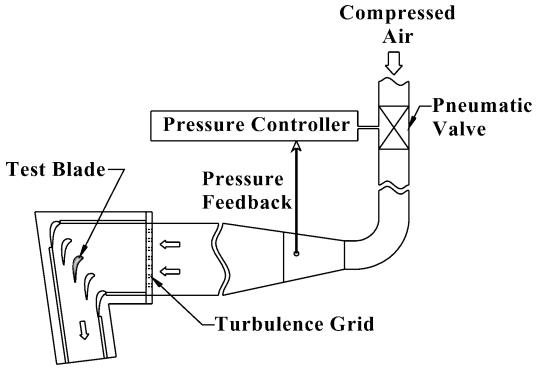

Fig. 1 Schematic of test section and blowdown facility.

0.5, 1.0, and 2.0. The experimental data have also been compared to numerical predictions from a commercial computational-fluid-dynamics (CFD) code mainly to understand the flowpath of the coolant and its interaction with the mainstream. Numerical investigations were performed using Fluent by resolving the domain into about 1.5 million grid points. The experimental results for pressure and effectiveness will aid future engineers to design more efficient turbine blades and help to calibrate CFD codes.

Experimental Setup

The test section consisted of a five-blade linear cascade with blade-tip profiles placed in a blowdown loop. A schematic of the test section and the blowdown loop is shown in Fig. 1. Inlet cross section of the test section was 31.1 cm (width) × 12.2 cm (height). A turbulence-generating grid (rectangular bar mesh type) with a porosity of 57% was placed before the inlet. Turbulence intensity was recorded 6 cm upstream of the middle blade (or 20.7 cm downstream of the grid) using a hot-wire probe. Turbulence intensity Tu at this location was found to be 9.7% because of the presence of the grid, and turbulence length scales were estimated to be 1.5 cm, which is slightly larger than the grid bar size. The bottom and sides on the test section were machined out of 1.27-cm-thick polycarbonate sheets, whereas a 1.27-cm-thick acrylic plate was used for the top for better optical access to the blade tip. The top plate also acted as a shroud for the blades. A 12-bit, scientific grade charge-coupled-device (CCD) camera, which could maintain a constant CCD temperature (−15°C), was mounted above the test section and was used to record the images. Flow conditions in adjacent passages of the center blade were ensured to be identical by adjusting the trailing-edge tailboards for the cascade. A comprehensive discussion on the flow conditions, including flow periodicity in the cascade and pressure distribution along the blade, has been reported by Azad et al.[13,14] and Kwak and Han.[18,19]

During the blowdown test, the cascade inlet air velocity and exit velocity were 80 and 220 m/s, respectively. The Reynolds number based on the axial chord length and exit velocity was 1.48×10^6. Overall pressure ratio (P_t/P) was 1.28 (where P_t is inlet total pressure and P is exit static pressure), and inlet and exit Mach numbers were 0.23 and 0.65, respectively. The pressure ratio and exit Mach number are higher than those reported by Kwak and Han.[18,19] The blowdown facility could maintain steady flow in the cascade for about 40 s. Compressed air stored in tanks entered a high flow pneumatic control valve, which could maintain steady flow by receiving downstream pressure feedback. The control valve could maintain a velocity within ± 3% of desired value.

A 3X scaled model of the GE-E^3 blade was used with a blade span of 12.2 cm and an axial chord length of 8.61 cm. Because the blades were placed in a linear cascade, they were machined for a constant cross section for its entire span corresponding to the tip profile of the actual GE-E^3 blade. Figure 2 shows the blade profiles, the inlet and exit angles for air, and the blade tip and shroud definitions. The test blade was made using stereolithography as conventional machining methods were unsuitable for such a complicated geometry. The four guide blades placed in the test section were made of aluminum. Figure 3 shows the film-cooling measurement blade with the internal passage geometry. The passages are numbered from 1 to 6 with passage 1 closest to leading edge and passage 6 closest to trailing edge. A squealer tipped blade with a recess of 4.22% of blade span (0.508 cm) was used. Coolant was supplied to the test blade through two loops with three serpentine passages with a 3-mm wall thickness in each loop as shown. The design of the passages was based on the E3, stage 1, HPT rotor-blade cooling system as discussed by Halila et al.[35] The leading-edge impingement wall in their design was removed to simplify the passage flow analysis. Figure 4 shows the geometry and orientation of the film-cooling holes on the pressure side and on the squealer blade tip. Eight cylindrical tip holes with a diameter of 1.1 mm ($L/d = 5.78$) were provided on the tip

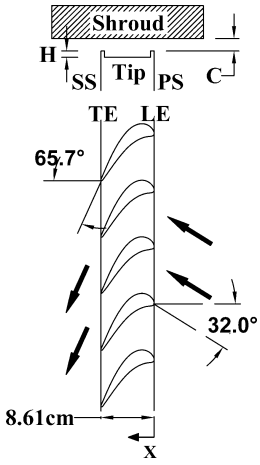

Fig. 2 Definition of blade tip and shroud.

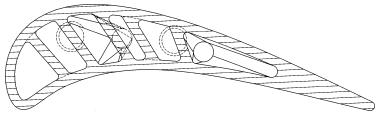

a) Section view at midspan

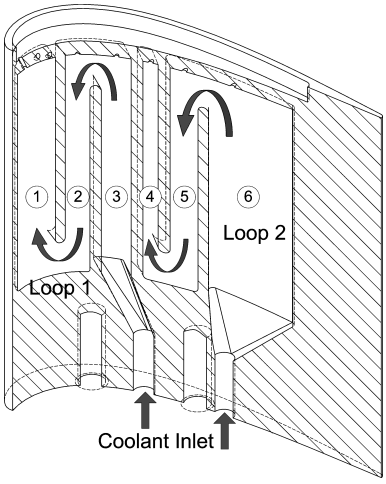

b) Section view along Camber Line

Fig. 3 Internal passage geometry of test blade.

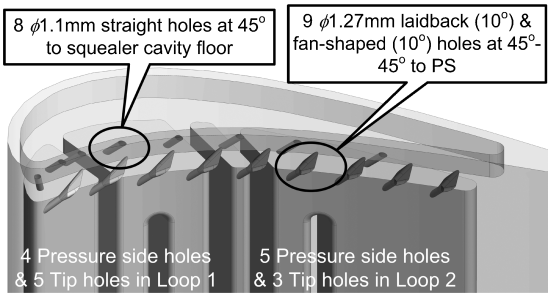

Fig. 4 Orientation of tip and pressure-side (PS) holes.

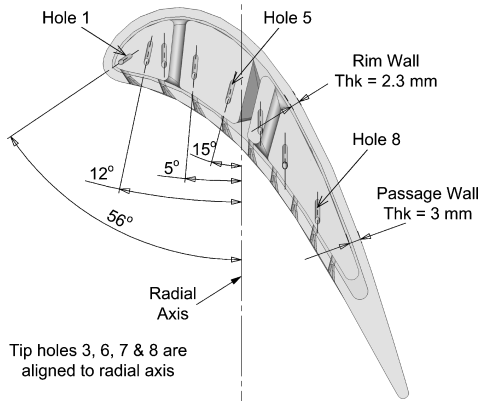

Fig. 5 Tip hole orientation.

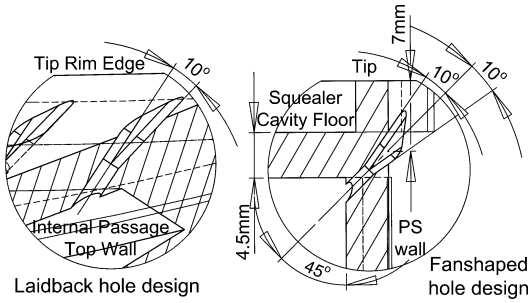

Fig. 6 Detail geometry of *PS*-shaped hole.

such that they break out along the camber line of the blade on the internal passage top wall. The thickness of the wall between the internal passages and the cavity floor was 0.45 cm. Figure 5 shows tip hole orientation with respect to the radial axis. The first tip hole near the leading edge was drilled at 60 deg to the cavity floor giving a length of diameter ratio (L/d) of 4.7. The remaining seven holes were drilled at 45 deg to the cavity floor with an $L/d = 5.8$. The angles with respect to the radial axis are shown in Fig. 5. The location and arrangement of the tip holes was similar to that described by Halila et al.[35] for the HP turbine rotor blade. The first five tip holes were connected to loop 1 (near the leading edge) and the remaining three to loop 2 (near the trailing edge). Nine film-cooling holes with a diameter of 1.27 mm and a hole spacing of 0.89 cm were provided for coolant to pass through on the airfoil pressure side. The pressure-side holes were located 0.7 cm below the tip surface at a compound angle of 45 deg to the blade span and 45 deg with respect to the airfoil pressure surface with $L/d = 4$. Figure 6 shows the detail views of the shaped holes. A laidback and fan-shaped design was employed for these nine holes with the holes expanding by 10 deg in the three directions (10-10-10) with the expansion starting from the middle of the hole length. The complete blade geometry including the blade profiles, cooling holes and passage design can be provided by the authors to researchers or turbine-blade designers for CFD validation.

This study was performed for a tip gap of 1.5% of blade span (12.2 cm), which was maintained on the middle three blades. Coolant injection through tip and pressure-side holes *TP* as well as pressure-side holes *P* only was studied. Experiments were performed with three different average blowing ratios M of 0.5, 1.0, and 2.0. During testing, it was observed that actual velocity of the leakage flow and coolant air could vary with the location and mass flow rate of the coolant. For this reason, the average blowing ratio was defined as $M = \rho_c V_c / \rho_m V_{\text{avg}}$. If the density is same, the ratio is reduced to a velocity ratio.

Discharge Coefficients and Local Blowing Ratios

The discharge coefficients, C_D as discussed by Gritsch et al.,[36] were assumed to be the constant for all open holes in a loop for tip and pressure-side coolant injection (*TP* cases) as well as only pressure-side coolant injection (*P* cases). Figure 7 shows average

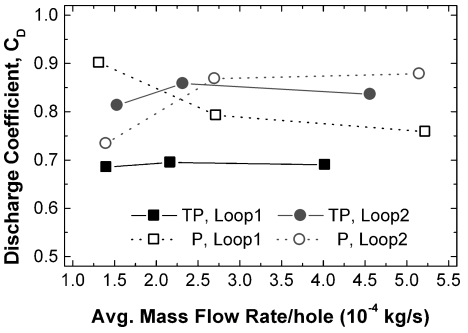

Fig. 7 Average C_D for *TP* and *P* cases.

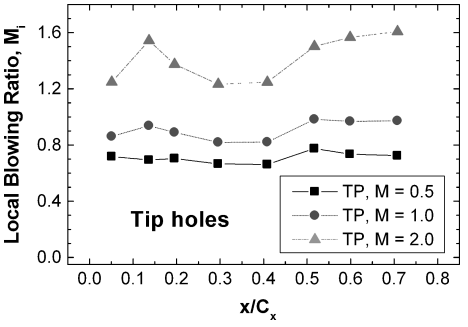

Fig. 8 Local M for tip holes for *TP* cases.

discharge coefficients for each loop for *TP* and *P* cases as calculated by using Eq. (1). It can be observed that for *TP* cases C_D is higher for loop 2 as compared to loop 1. This could be because of the presence of four shaped holes on pressure side and five straight holes on the tip for loop 1, whereas for loop 2 there are five shaped holes on the pressure side and three straight holes on the tip. The discharge coefficient for shaped holes is higher, which results in a higher average C_D value for loop 2. Discharge coefficients for shaped holes (*P* cases) are high with an average value of 0.82. The constant C_D assumption for all holes in the loop might not be true as C_D depends on not only the geometry but also the external and internal flow conditions. Average C_D values just provide a representative means to understand the coolant flow through the film-cooling holes. By knowing total mass flow rate of the coolant, discharge coefficient, and pressure differential for each hole, the local blowing ratio M_i was calculated:

$$C_D = \dot{m}_{\text{hole}} \Bigg/ \Bigg\{ \left(\frac{\pi}{4} d^2\right) \left[P_{\text{t,passage}} \left(\frac{P_{\text{blade}}}{P_{\text{t,passage}}} \right)^{(\gamma+1)/2\gamma} \right] \sqrt{\frac{2\gamma}{(\gamma-1) R T_c} \left[\left(\frac{P_{\text{t,passage}}}{P_{\text{blade}}} \right)^{(\gamma-1)/\gamma} - 1 \right]} \Bigg\} \tag{1}$$

To better explain the results for effectiveness, local blowing ratios through each hole on the tip and airfoil pressure side have been plotted in Figs. 8 and 9, respectively. Local mass flux on the surface of the blade was found using the inlet total pressure and local static pressure. The local surface static-pressure distribution for the tip was found using PSP, whereas static-pressure taps located at 97% of blade span were used to measure static pressure on the near-tip pressure side. The static pressure in the passages inside the blade was measured using 14 static pressure taps on the pressure- or suction-side inner passage wall located 3.18 mm below the passage top wall. Local blowing ratio was calculated by using the pressure differential for each hole.

From Fig. 8, for coolant injection for tip holes, the blowing ratio shows a more or less uniform distribution with slightly lower values for the fourth and fifth holes. This is mainly caused by lower passage pressure in the turn region from passage 3 to 2. Pressure in passage 1

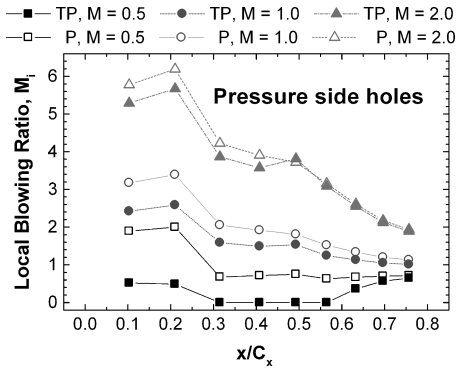

Fig. 9 Local *M* for *PS* holes for *TP* and *P* cases.

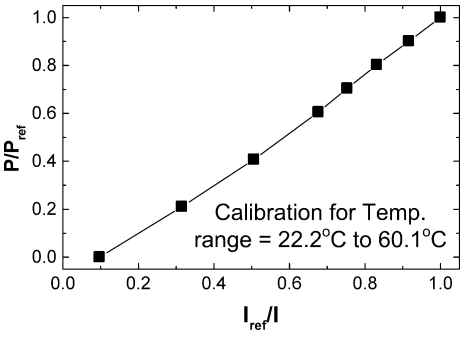

Fig. 10 Calibration curve for PSP.

closest to leading edge is higher because of stagnation of the coolant causing slightly higher local blowing ratio for tip holes 1, 2, and 3. This also results in a high local blowing ratio for the first two pressure-side holes located on passage 1 as can be observed from Fig. 9. The local blowing ratio gradually decreases with increasing chord because of the increase in the mainstream mass flux on the pressure side as the flow approaches the throat region. A nonuniform coolant distribution exists between the tip and pressure-side holes for *TP* cases. The average coolant mass flow per hole through the pressure-side holes is higher for higher blowing ratios as compared to tip holes, but at lower blowing ratios average coolant mass flow per hole is higher for tip holes.

Film-Cooling Effectiveness Measurement Theory and Data Analysis

PSP was used to measure the film-cooling effectiveness on the blade tip. PSP technique has also been used by other researchers to measure film-cooling effectiveness. Zhang et al.[37] conducted experimental work by applying PSP technique to measure the local film-cooling effectiveness distribution on a turbine nozzle endwall by using air and nitrogen as coolants. The accuracy of this technique for measuring film-cooling effectiveness has been compared by Wright et al.[38] on a flat plate with compound angled ejection holes using steady-state infra-red (IR) technique and steady state temperature sensitive paint (TSP) technique. Results were obtained for a range of blowing ratio and show reasonable agreement with each other with IR, TSP as well as PSP giving effectiveness results within 15% of each other. Larger uncertainties for heat transfer techniques such as IR and TSP methods were observed due to lateral heat conduction in the flat plate as corrections for heat conduction were not included in the presented results.

PSP is a photoluminescent material that emits light with intensity proportional to the surrounding partial pressure of oxygen. Any pressure variation on the PSP-coated surface causes emitting light intensity to change as a result of an oxygen-quenching process. A CCD camera measures this change of intensity. A calibration performed for intensity ratio to give pressure ratio gives pressure information. To measure the film-cooling effectiveness and to obtain the intensity ratio from PSP, four kinds of images are required: a reference image (with illumination, no mainstream flow, surrounding pressure uniform at 1atm), an air image (with illumination and mainstream flow, air used as coolant), an air/nitrogen image (with illumination and mainstream flow, nitrogen gas used as coolant), and a black image (no illumination and no mainstream and coolant flow) to remove noise effects from the camera.

Oxygen partial pressure information is obtained from the intensity ratio and calibration curve. This oxygen partial pressure information can be directly converted into static-pressure distribution for the case with air coolant injection. Intensity ratio for air and air/nitrogen mixture is calculated using Eqs. (2) and (3), respectively.

$$\frac{I_{\text{ref}} - I_{\text{blk}}}{I_{\text{air}} - I_{\text{blk}}} = func\left[\left(P_{\text{O}_2}\right)_{\text{air}}\right] \quad \text{or} \quad func(P) \tag{2}$$

$$\frac{I_{\text{ref}} - I_{\text{blk}}}{I_{\text{mix}} - I_{\text{blk}}} = func\left[\left(P_{\text{O}_2}\right)_{\text{mix}}\right] \tag{3}$$

where I denotes the intensity obtained for each pixel for reference (ref), black (blk), air and air/nitrogen (mix) images, and $func(P)$ is the relation between intensity ratio and pressure ratio obtained after calibrating the PSP. $(P_{\text{O}_2})_{\text{air}}$ and $(P_{\text{O}_2})_{\text{mix}}$ are the partial pressures of oxygen on the test surface for air and air/nitrogen mixture images, respectively.

The film-cooling effectiveness can be expressed as a ratio of oxygen concentrations measured by PSP and is calculated using the following equation:

$$\eta = \frac{Co_{\text{air}} - Co_{\text{mix}}}{Co_{\text{air}}} = \frac{(P_{\text{O}_2})_{\text{air}} - (P_{\text{O}_2})_{\text{mix}}}{(P_{\text{O}_2})_{\text{air}}} \tag{4}$$

where Co_{air} 15 and Co_{mix} are the oxygen concentrations of mainstream air and air/nitrogen mixture on the test surface, respectively. By assuming the molecular weights of air and nitrogen as the same, effectiveness can be expressed as a ratio of partial pressures of oxygen due to proportionality between concentration and partial pressure.

The PSP-coated blade tip was illuminated by a strobe light fitted with an optical filter. Light emerging from this filter was green light with a center wavelength of 520 nm and a bandwidth of 20 nm. A 12-bit scientific-grade CCD camera (high-speed Sensicam with CCD temperature maintained at -15°C using two-stage peltier cooler) with an exposure time of 1 ms was employed to measure emitting light intensity. An optical 610-nm long-pass filter was placed in front of the camera to record red light emitted from the PSP. Optical filters were chosen to match the wavelengths for excitation (green) and return (red) signals for the PSP. Special care was taken in choosing the wavelength range of the filters to avoid any overlap of the ranges, so that the camera could detect only the excited light from PSP and not the reflected light from the light source. The camera and the strobe light were triggered at the same time by a 20-Hz trigger signal. The image resolution obtained from the camera was 1.41 pixels/mm.

The PSP-coated blade-tip surface was constructed by layering it with PSP using an airbrush. Calibration for the PSP was conducted inside a vacuum chamber. Air was removed from the chamber by a vacuum pump, and the intensity from the PSP-coated test plate was recorded at different pressures ($P < P_{\text{ref}} = 1$ atm). Pressure was varied from 0 to 1 atm. The same optical components, strobe light and camera, were used in the calibration. There is a temperature dependency of PSP. However, if the intensity is normalized by that of the reference image (at 1 atm), the calibration curves, at different temperatures, fall into one curve. Figure 10 shows the calibration curve of intensity ratio vs pressure ratio. During testing, it was ensured that temperatures of mainstream air, coolant, and test section were the same while taking reference, air, and nitrogen images to minimize uncertainty. Thermocouples (T-type) located upstream of the test section and in the coolant flow recorded temperatures of air and nitrogen gas. Experiments were conducted in an air-conditioned room (20°C), and temperatures of mainstream air, coolant air, and nitrogen gas were maintained at 20°C.

Coolant mass flow to each loop was set using two separate Rotameters to a flow rate corresponding to the blowing ratio. A pneumatic valve was opened, and the pressure controller was set to the desired flow rate for the mainstream air. A function generator was used to generate transistor transistor logic (TTL) trigger signal for camera and strobe light. The images were taken when the mainstream flow was fully developed, that is, after the initial developing time for flow (~15 s). After the images were captured, the pneumatic valve was closed. The duration of a single experiment was about 30 s.

Images obtained from the camera were saved, and a program created to calculate the average intensity value at each image pixel was executed. Two-hundred images (10 s at 20 Hz) were captured for each case, and the average pixel intensity was calculated from these images. Another program was used to convert the intensity magnitudes to partial pressure of oxygen and then to film-cooling effectiveness. Results obtained for each pixel were plotted as contour plots and are presented.

Uncertainty calculations were performed based on a confidence level of 95% and are based on the uncertainty analysis method of Coleman and Steele.[39] Lower effectiveness magnitudes have higher uncertainties. For an effectiveness magnitude of 0.3, uncertainty was around 2%, whereas for an effectiveness magnitude of 0.07 uncertainty was as high as 10.3%. Uncertainties for very low effectiveness magnitudes can be higher. This uncertainty is the result of uncertainties in calibration (4%) and image capture (1%). Uncertainties for the blowing ratios are estimated to be 4%.

Computational Methodology

Computations were performed for the blade-tip flow and film cooling for the same blade-tip geometry using a commercial software package FLUENT. This code solves compressible Reynolds-averaged Navier–Stokes equations using the finite volume method to discretize the equations. The GAMBIT grid-generation software was used to generate unstructured tetrahedral grids, with fine-grid clustering in the near-wall and tip film-cooling regions. Numerical study has been undertaken primarily to understand the flowpath of the coolant and its interaction with the mainstream and also to calibrate the CFD code by comparing with experimental data. Numerical predictions were made only for *TP* cases.

The computational domain consisted of a single blade with periodic conditions imposed along the boundaries in the circumferential (pitch) direction. The inlet boundary was placed at one-half chord length upstream of the blade so that the simple uniform inflow boundary conditions could be employed. The total temperature (293 K) and total pressure (147.39 kPa) were specified along with the inlet flow angle (32 deg) and turbulence intensity level (9.7%). The corresponding Mach number at the inlet was 0.25. The exit boundary was located at one chord length downstream of the blade trailing edge to provide appropriate resolution of the tip leakage flow and passage vortices. On the blade surface, a no-slip condition with adiabatic temperature was specified. The coolant temperature was set 50°C higher than the mainstream so that adiabatic effectiveness could be calculated.

For blade-tip leakage flow and heat-transfer simulations, Yang et al.[30,31] have showed that the Reynolds-stress model of Hanjalic[40] performed slightly better than the high-Reynolds-number k–ε model[41] and renormalization group (RNG) k–ε model.[40] In all cases, a nonequilibrium wall function was employed to handle the near-wall turbulence. The y^+ value is adjusted iteratively to about 30 by splitting or merging the near-wall grids to satisfy the requirement of nonequilibrium wall function. All of the cases presented converged to residual levels of the order of 10^{-5} and to less than 0.01% error in the mass flow rate between the inlet and exit of the computational domain. About 1.5 million nodes were applied in these calculations with the grid resolution based on the grid-independence study performed by Yang et al.[30,31] Typically, 1000 iterations were required for convergence.

Film-Cooling Effectiveness Results

Pathlines of the coolant colored with dimensionless temperature θ obtained from numerical predictions are shown in Fig. 11 on the blade tip and inside the serpentine passages. Rapid change in coolant temperature can be observed as it comes into contact with the mainstream flow. The 180-deg turning effect in the serpentine passages can also be noticed on the flowpath of the coolant. Large recirculating zones can be spotted in passages 1 and 6 as a result of the flow orientation and their large cross-section area.

Film-Cooling Effectiveness Results for Tip and Pressure-Side Coolant Injection (*TP*)

Figure 12 shows film-cooling effectiveness distribution for a squealer blade tip for coolant flow from tip as well as from the pressure-side holes. The first row in the figure shows the result on the tip for the three blowing ratios of $M = 0.5$, 1.0, and 2.0 arranged in column-wise fashion while the second row shows the effectiveness data obtained on the near-tip pressure side.

Film-cooling effectiveness is found to increase with increasing blowing ratio on the tip. It can be discerned from the contour plots from Fig. 12 that the coolant trace from the tip holes moves towards the pressure-side trailing edge. This is probably because of a recirculation zone induced by the squealer rim. Presence of this recirculation zone can be confirmed in Fig. 13, which shows the

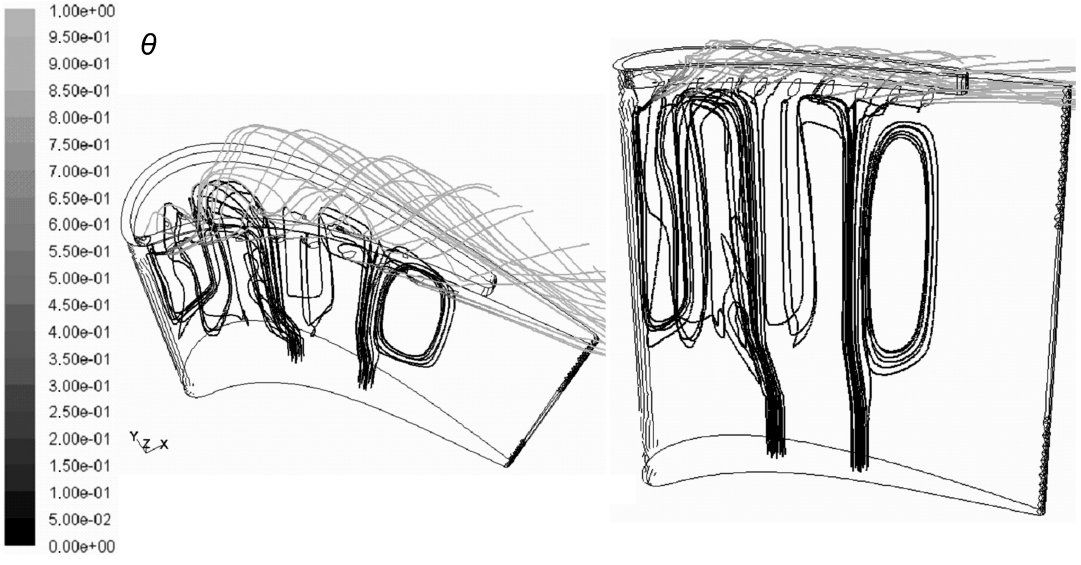

Fig. 11 Numerical predictions of coolant pathlines on the blade tip and inside the coolant loops colored with dimensionless temperature.

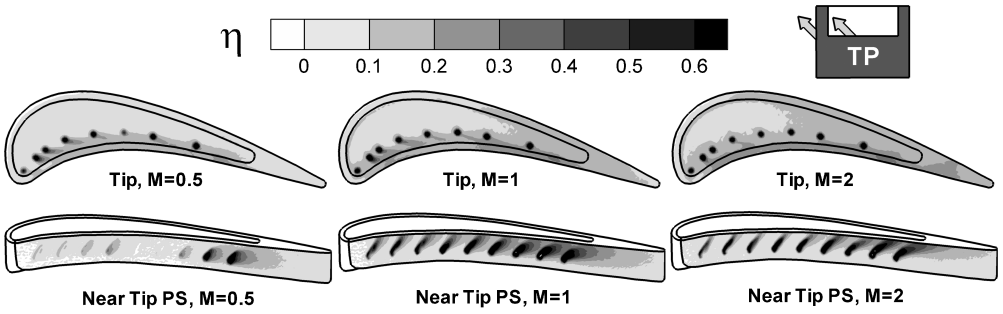

Fig. 12 Film-cooling effectiveness distribution on tip and near-tip pressure side for *TP* cases.

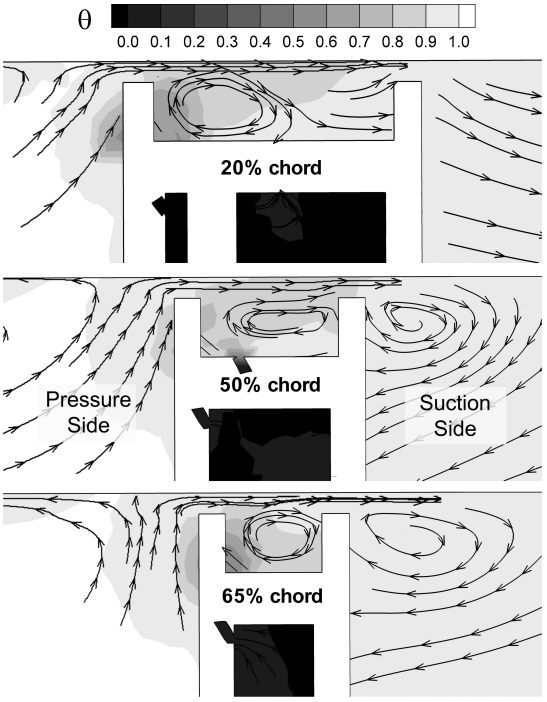

Fig. 13 Stream vectors along with dimensionless temperature contours for three cross sections along tip.

stream vectors of the flow as obtained from numerical predictions for $M = 1$ along with the dimensionless temperature θ at three different cross sections on the blade tip cut normal to the chord with the first cutting plane closer to the leading edge (20% chord), the second in the middle (50% chord), and the third closer to the end of the cavity near the trailing edge (65% chord). Development of the tip vortex on the suction side can also be discerned from the stream vectors. Lower temperatures caused by mixing of the colder jet with the mainstream can be observed near the pressure-side inner and outer rim walls implying good film coverage.

From Fig. 12, effectiveness immediately downstream of the tip holes is very high with the magnitude dropping rapidly further downstream. Liftoff of the jets can be observed for the holes on loop 2 (tip holes 5, 6, 7, and 8) for higher blowing ratios while higher effectiveness magnitudes downstream of the holes on loop 1 can be observed as the coolant jets stay closer to the cavity surface. Some coolant coverage can also be observed on the cavity floor towards the suction-side/trailing-edge inner rim wall. This is probably because of some coolant being trapped and recirculated inside the squealer cavity. The pressure-side rim shows relatively high effectiveness magnitudes as a result of carryover of the pressure-side coolant. Some coolant shooting from the tip holes for high blowing ratios can also penetrate the mainstream leakage flow to provide additional film coverage on the pressure side rim. Some traces can also be observed near the trailing edge and on the suction-side rim. The effectiveness magnitudes immediately downstream of the tip holes show higher magnitudes as compared to Ahn et al.[6] They presented data with coolant injection at 90 deg to the blade-tip surface, which is more prone to dilution with the mainstream flow, thus lowering effectiveness. In the present study, coolant is injected at 45 deg to the blade-tip surface. Though the contour levels show a maximum effectiveness of only 0.6, the effectiveness in the hole and near hole region is very high. Magnified views for three tip holes and three pressure-side holes are shown in Fig. 14 for $M = 1$. Effectiveness inside the hole was recorded to be about 0.9. Liftoff of the coolant jet can be noted for tip holes 5 and 8, indicating that the high jet momentum causes direct impingement on the pressure-side inner rim wall. The sudden decrease in effectiveness immediately downstream of these holes is a result of the coolant jet losing contact with the cavity surface indicating liftoff.

Numerical prediction of the results for the same cascade flow conditions and the three blowing ratios is presented in Fig. 15. The first row shows numerical results on the tip while the second row shows the predictions on the near-tip pressure side. Film-cooling effectiveness on the inner rim walls is also shown in the third row. The numerical predictions show similar trends as experimental results. Figures 12 and 15 are plotted for the same contour level. Relatively good comparisons for the tip can be observed for $M = 0.5$ and 1. The effectiveness levels from numerical simulation for $M = 2$ though are found to be higher. These higher magnitudes can be caused by an inability of the CFD code to capture the flow unsteadiness of the high-momentum jet around the hole region leading to less mixing of the coolant with the mainstream.

Film-cooling effectiveness on the pressure side is very low for the holes near midchord region for $M = 0.5$. Nearly equal pressures in the passage and on the outer blade surface cause very little coolant to come out through these holes. The last two pressure-side holes though show much higher effectiveness because of lower static pressures on the blade surface. More spreading of the coolant coming from the last four holes can be observed for $M = 1$ as compared to $M = 2$ resulting in higher effectiveness. For $M = 2$, the high-momentum coolant jet shoots towards the tip gap with little spreading. On the other hand, coolant coming out from the first five pressure side holes for $M = 1$ and 2 show little spreading and relatively lower effectiveness owing to liftoff of the jet from the surface because of very high local blowing ratios for these holes. Magnified views for pressure-side holes 2, 5, and 8 shown in Fig. 14 visibly indicate the bending of the coolant jet as a result of decreasing local blowing ratio as the mainstream flow moves towards the trailing edge. When compared to results from CFD analysis (Fig. 15), for a blowing ratio of 1, there is good agreement between the two sets of data. For $M = 0.5$ and 2 though, the CFD code used overpredicts the effectiveness magnitudes. Some effectiveness was observed upstream of the pressure-side holes by Mhetras et al.[42] for higher blowing ratios, which is unusual. This can be because of reflection error on the near-tip PS surface. In the present study, the test blade was first coated with a nonreflective black paint before layering it with PSP to minimize light reflection from the test surface.

Film-cooling effectiveness results for the pressure-side inner rim wall and suction-side inner rim wall have been shown in Fig. 16. The tip film-cooling holes are designed so that the high-momentum coolant jet will impinge on the pressure-side inner rim wall. Coolant

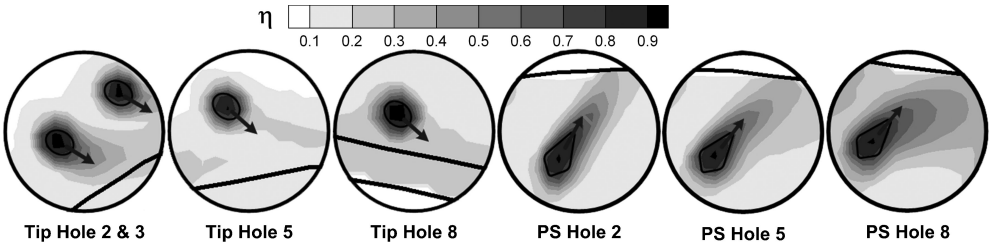

Fig. 14 Magnified view of effectiveness levels near some typical tip and *PS* holes for $M = 1$ for *TP* case.

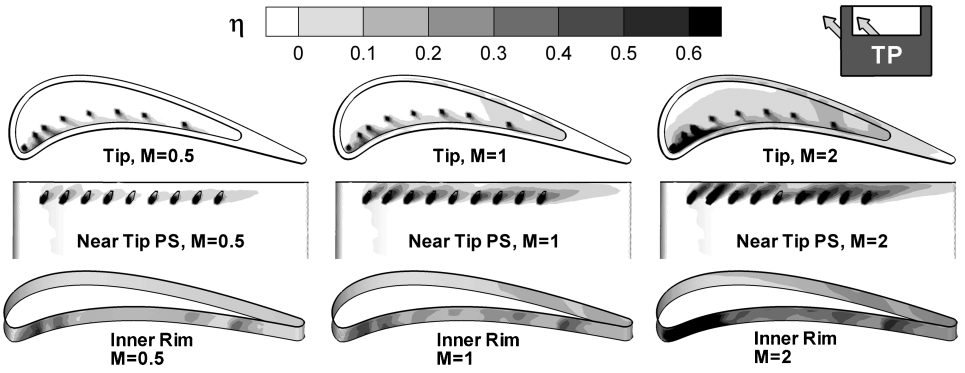

Fig. 15 Numerical predictions for film-cooling effectiveness on tip, near-tip *PS*, and inner cavity rim walls for *TP* cases.

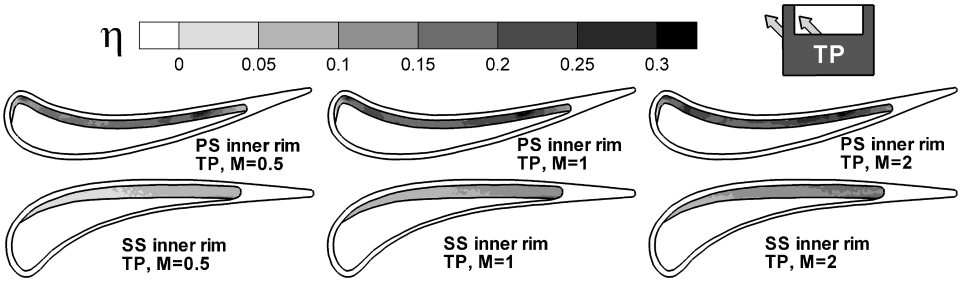

Fig. 16 Film-cooling effectiveness distribution on inner rim walls for *PS* and Suction Side (SS) for *TP* cases.

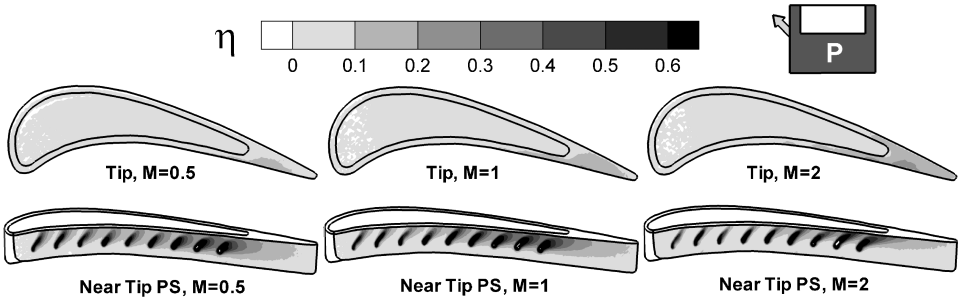

Fig. 17 Film-cooling effectiveness distribution on tip and near-tip pressure side for *P* cases.

jets will remove heat from the tip rim wall by increasing the heat-transfer coefficients. Additional coolant coverage will decrease the surface temperature difference by preventing the mainstream hot gas coming into contact with the blade tip. Almost uniform film coverage is obtained on the pressure-side inner rim wall with effectiveness magnitudes increasing with higher blowing ratios. Higher magnitudes ($\sim$0.25) can be observed where the coolant jet impinges on the rim wall. Some remnants of the coolant can also be discerned from traces on the suction-side inner rim wall, which can be attributed to some coolant from the tip holes getting trapped inside the recirculation vortex in the squealer cavity. Similar observations can be made from the numerical predictions indicating that CFD code is able to capture the flow physics inside the cavity. The effectiveness magnitudes compare well for $M = 0.5$ and 1, whereas they are overpredicted for $M = 2$ especially on the pressure-side inner rim close to the leading edge.

Film-Cooling Effectiveness Results for Only Pressure-Side Coolant Injection (*P*)

Figure 17 depicts the contour plots for effectiveness obtained on the tip and on the near-tip pressure side, whereas Fig. 18 shows the effectiveness plots for the inner rim walls for three blowing ratios with coolant injection through only pressure-side shaped holes. The tip holes were sealed for these cases. From Fig. 17, some traces of coolant can be observed on the cavity floor of squealer tip for blowing ratios of 1 and 2 near the trailing-edge side. This could be caused by entrainment of the coolant coming from the pressure side into the recirculating vortex region. The effectiveness magnitudes though are very low ($\sim$0.1). Some coolant traces can also be discerned on the pressure-side rim, which is caused by the coolant carrying over into the tip gap. Higher effectiveness magnitudes can be noted near the trailing-edge rim. Effectiveness magnitudes though are generally much lower than those for *TP* cases.

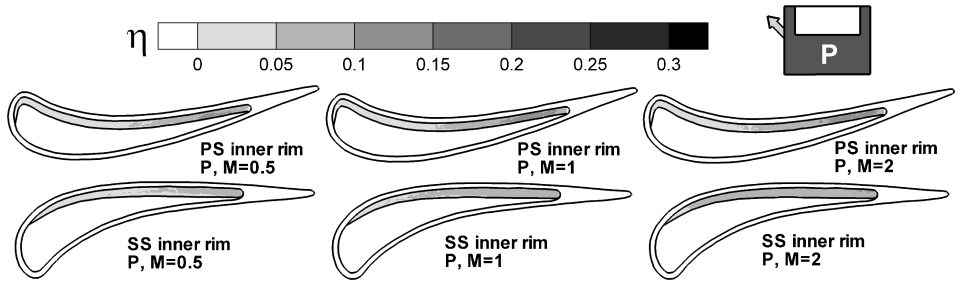

Fig. 18 Film-cooling effectiveness distribution on inner rim walls for PS and SS for *P* cases.

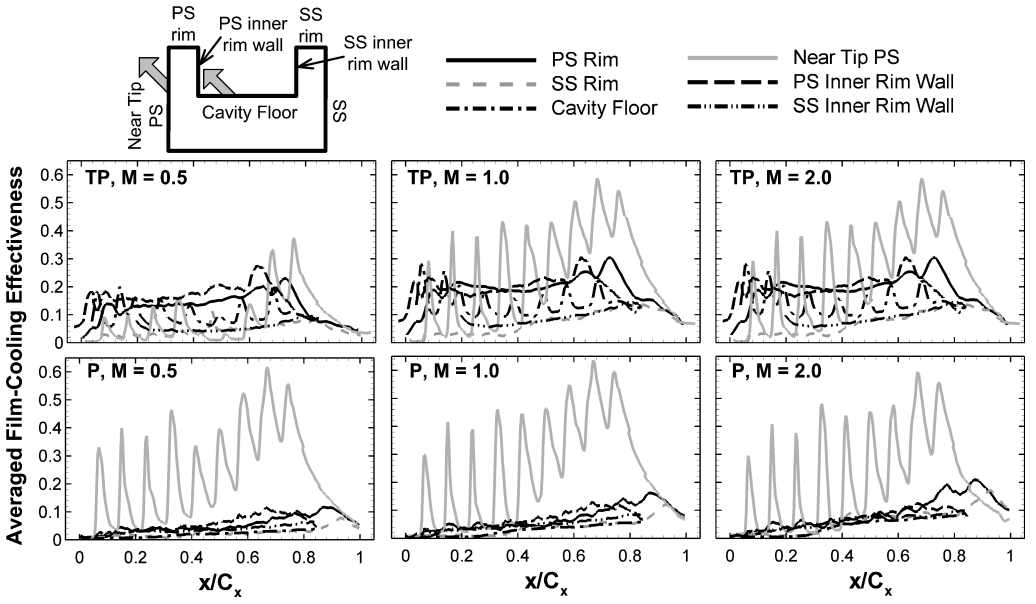

Fig. 19 Averaged film-cooling effectiveness from experimental results for all cases.

As observed for *TP* cases, more spreading of the coolant can be observed for $M = 1$ on the near-tip pressure side as compared to $M = 0.5$ and 2 for holes near the trailing edge. Weaker jet momentum from these holes for $M = 0.5$ restricts the spreading of the coolant. The effectiveness on the pressure side though is much higher for $M = 0.5$ as compared to *TP* case mainly because in the latter case more coolant was diverted to the tip holes. This effect can also be discerned from the local blowing ratio plot in Fig. 9. $M = 0.5$ shows more spreading near the first few holes close to the leading edge than $M = 1.0$ and 2.0. High-momentum jets for $M = 2.0$ on the other hand do not smear as much as for $M = 0.5$ and 1.0 resulting in a relatively straighter coolant trace. Liftoff of the coolant jet can also be observed for the holes closer to the leading edge and mid-chord. This effect is similar to that observed for *TP* cases and can be attributed to the very high local blowing ratios for these holes. Some minor traces of the coolant can also be observed for the inner rim walls from Fig. 18 on the pressure and suction side of the squealer cavity with higher magnitudes for higher blowing ratios.

Averaged Film-Cooling Effectiveness Results

Figure 19 shows the variation of averaged film-cooling effectiveness along the axial chord for the plane and squealer blade tip for all cases. The averaged values are obtained by averaging the effectiveness magnitudes at a given x/C_x location. For the near-tip pressure-side holes, the averaged results were obtained by averaging from the base of the hole to the tip. Data are shown for all six surfaces for each case. The trends indicate that effectiveness increases with blowing ratio. High peak values for effectiveness can be noted for the near-tip pressure-side surface with each spike representing the presence of a hole. This is mainly because of higher effectiveness on this surface as a result of the presence of shaped holes. The peak values near the hole locations on the cavity floor though are much lower as the area closer to the suction-side inner rim wall shows

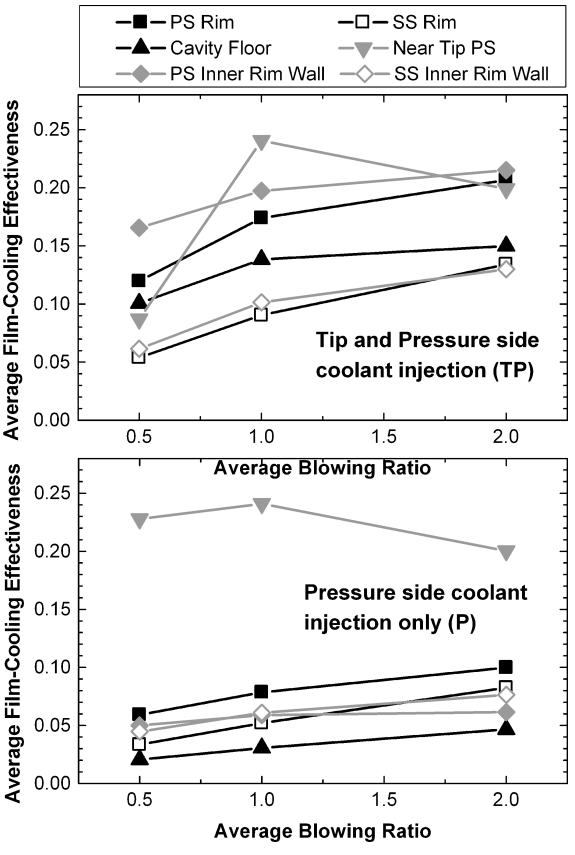

Fig. 20 Area averaged film-cooling effectiveness.

low effectiveness magnitudes. Hence, after averaging, the peak values are muted. Almost uniform effectiveness of about 0.2 can be observed for the pressure-side rim and inner wall for *TP* cases. For *P* cases, effectiveness values are very low (< 0.1) for the cavity floor and inner rim walls. Average values for the near-tip holes are similar to those for *TP* case. Figure 20 shows the area-averaged film-cooling effectiveness results. For the near-tip pressure side, a blowing ratio of $M = 1$ shows best performance for *TP* and *P* cases as a result of spreading of the coolant. For the other surfaces on the tip though, $M = 2$ shows highest effectiveness.

Conclusions

A parametric study has been performed for measuring film-cooling effectiveness on a squealer blade tip. Effectiveness was measured on the cavity floor, rim, cavity rim walls, and near-tip pressure side. Effects of coolant injection from pressure side and tip and pressure side and varying blowing ratio have also been studied. Major findings from the experimental and numerical results are listed next.

1) In general, higher blowing ratios give higher effectiveness on the tip rim, cavity floor, and inner rim walls. For the near-tip pressure side, $M = 1$ shows best results.

2) The pressure-side rim and inner and outer squealer rim walls show high and uniform effectiveness because of the combined effect of tip and pressure-side coolant injection.

3) Entrainment of coolant in the squealer cavity recirculation vortex can help in providing film coverage on the suction side rim and inner rim wall.

4) Coolant injection from only pressure side gives poor film-cooling performance on the cavity floor and inner rim walls.

5) Presence of serpentine passages to supply coolant to the holes results in a large variation of local blowing ratios, which can have a significant impact on film-cooling performance.

6) Greater control of local blowing ratios for holes on the near-tip pressure side can provide more uniform film coverage.

Acknowledgments

This work was prepared with the partial support of National Science Foundation under Grant CTS-9903972 and State of Texas Advanced Technology Program. This paper was presented at the ASME IGTI 2005 Conference (Paper Number GT2005-68387).

References

[1]Han, J. C., Dutta, S., and Ekkad, S. V., *Gas Turbine Heat Transfer and Cooling Technology*, 1st ed., Vol. 1, Taylor and Francis, New York, 2000, Chaps. 2, 3.

[2]Kim, Y. W., and Metzger, D. E., "Heat Transfer and Effectiveness on Film Cooled Turbine Blade Tip Model," *Journal of Turbomachinery*, Vol. 117, No. 1, 1995, pp. 12–21.

[3]Kim, Y. W., Downs, J. P., Soechting, F. O., Abdel-Messeh, W., Steuber, G. D., and Tanrikut, S., "A Summary of the Cooled Turbine Blade Tip Heat Transfer and Film Effectiveness Investigations Performed by Dr. D. E. Metzger," *Journal of Turbomachinery*, Vol. 117, No. 1, 1995, pp. 1–11.

[4]Kwak, J. S., and Han, J. C., "Heat Transfer Coefficient and Film-Cooling Effectiveness on a Gas Turbine Blade Tip," American Society of Mechanical Engineers, Paper GT-2002-30194, June 2002.

[5]Kwak, J. S., and Han, J. C., "Heat Transfer Coefficient and Film-Cooling Effectiveness on the Squealer Tip of a Gas Turbine Blade," American Society of Mechanical Engineers, Paper GT-2002-30555, June 2002.

[6]Ahn, J., Mhetras, S. P., and Han, J. C., "Film-Cooling Effectiveness on a Gas Turbine Blade Tip," American Society of Mechanical Engineers, Paper GT-2004-53249, June 2004.

[7]Christophel, J. R., Thole, K. A., and Cunha, F. J., "Cooling the Tip of a Turbine Blade Using Pressure Side Holes—Part 1: Adiabatic Effectiveness Measurements," American Society of Mechanical Engineers, Paper GT-2004-53251, June 2004.

[8]Christophel, J. R., Thole, K. A., and Cunha, F. J., "Cooling the Tip of a Turbine Blade Using Pressure Side Holes—Part 2: Heat Transfer Measurements," American Society of Mechanical Engineers, Paper GT-2004-53254, June 2004.

[9]Metzger, D. E., Dunn, M. G., and Hah, C., "Turbine Tip and Shroud Heat Transfer," *Journal of Turbomachinery*, Vol. 113, No. 3, 1991, pp. 502–507.

[10]Dunn, M. G., and Haldeman, C. W., "Time-Averaged Heat Flux for a Recessed Tip, Lip, and Platform of a Transonic Turbine Blade," *Journal of Turbomachinery*, Vol. 122, No. 4, 2000, pp. 692–697.

[11]Yang, T. T., and Diller, T. E., "Heat Transfer and Flow for a Grooved Turbine Blade Tip in a Transonic Cascade," American Society of Mechanical Engineers, Paper 95-WA/HT-29, Nov. 1995.

[12]Bunker, R. S., Baily, J. C., and Ameri, A. A., "Heat Transfer and Flow on the First Stage Blade Tip of a Power Generation Gas Turbine: Part 1: Experimental Results," *Journal of Turbomachinery*, Vol. 122, No. 2, 2000, pp. 272–277.

[13]Azad, GM. S., Han, J. C., Teng, S., and Boyle, R., "Heat Transfer and Pressure Distributions on a Gas Turbine Blade Tip," *Journal of Turbomachinery*, Vol. 122, No. 4, 2000, pp. 717–724.

[14]Azad, GM. S., Han, J. C., and Boyle, R., "Heat Transfer and Pressure Distributions on the Squealer Tip of a Gas Turbine Blade," *Journal of Turbomachinery*, Vol. 122, No. 4, 2000, pp. 725–732.

[15]Bunker, R. S., and Bailey, J. C., "Effect of Squealer Cavity Depth and Oxidation on Turbine Blade Tip Heat Transfer," American Society of Mechanical Engineers, Paper 2001-GT-0155, June 2001.

[16]Azad, GM. S., Han, J. C., Bunker, R. S., and Lee, C. P., "Effect of Squealer Geometry Arrangement on a Gas Turbine Blade Tip Heat Transfer," *Journal of Heat Transfer*, Vol. 124, No. 3, 2002, pp. 452–459.

[17]Kwak, J. S., Ahn, J., Han, J. C., Pang Lee, C., Bunker, R. S., Boyle, R., and Gaugler, R., "Heat Transfer Coefficients on Squealer Tip and Near Tip Regions of a Gas Turbine Blade with Single or Double Squealer," American Society of Mechanical Engineers, Paper GT-2003-38907, June 2002.

[18]Kwak, J. S., and Han, J. C., "Heat Transfer Coefficient on a Gas Turbine Blade Tip and near Tip Regions," *Journal of Thermophysics and Heat Transfer*, Vol. 17, No. 3, 2003, pp. 297–303.

[19]Kwak, J. S., and Han, J. C., "Heat Transfer Coefficient on the Squealer Tip and near Squealer Tip Regions of a Gas Turbine Blade," *Journal of Heat Transfer*, Vol. 125, No. 4, 2003, pp. 669–677.

[20]Mayle, R. E., and Metzger, D. E., "Heat Transfer at the Tip of an Unshrouded Turbine Blade," *Proceedings of the 7th International Heat Transfer Conference*, Hemisphere, New York, 1982, pp. 87–92.

[21]Heyes, F. J. G., Hodson, H. P., and Dailey, G. M., "The Effect of Blade Tip Geometry on the Tip Leakage Flow in Axial Turbine Cascades," American Society of Mechanical Engineers, 91-GT-135, June 1991.

[22]Teng, S., Han, J. C., and Azad, GM. S., "Detailed Heat Transfer Coefficient Distributions on a Large-Scale Gas Turbine Blade Tip," *Journal of Heat Transfer*, Vol. 123, No. 4, 2001, pp. 803–809.

[23]Papa, M., Goldstein, R. J., and Gori, F., "Effects of Tip Geometry and Tip Clearance on the Mass/Heat Transfer from a Large-Scale Gas Turbine Blade," *Journal of Turbomachinery*, Vol. 125, No. 1, 2003, pp. 90–99.

[24]Jin, P., and Goldstein, R. J., "Local Mass/Heat Transfer on a Turbine Blade Tip," HT-ABS-012, Feb. 2002.

[25]Jin, P., and Goldstein, R. J., "Local Mass/Heat Transfer on Turbine Blade near-Tip Surfaces," American Society of Mechanical Engineers, Paper 2002-GT-30556, June 2002.

[26]Saxena, V., Nasir, H., and Ekkad, S. V., "Effect of Blade Tip Geometry on Tip Flow and Heat Transfer for a Blade in a Low Speed Cascade," 2003-GT-38176, June 2003.

[27]Ameri, A. A., Steinthorsson, E., and Rigby, L. D., "Effects of Tip Clearance and Casing Recess on Heat Transfer and Stage Efficiency in Axial Turbines," *Journal of Turbomachinery*, Vol. 121, No. 4, 1999, pp. 683–693.

[28]Ameri, A. A., and Rigby, D. L., "A Numerical Analysis of Heat Transfer and Effectiveness on Film Cooled Turbine Blade Tip Models," NASA/CR 1999-209165, July 1999.

[29]Ameri, A. A., and Bunker, R. S., "Heat Transfer and Flow on the First Stage Blade Tip of a Power Generation Gas Turbine: Part 2: Simulation Results," *Journal of Turbomachinery*, Vol. 122, No. 2, 2000, pp. 272–277.

[30]Yang, H., Acharya, S., Ekkad, S. V., Prakash, C., and Bunker, R., "Flow and Heat Transfer Predictions for a Flat-Tip Turbine Blade," American Society of Mechanical Engineers, Paper 2002-GT-30190, June 2002.

[31]Yang, H., Acharya, S., Ekkad, S. V., Prakash, C., and Bunker, R., "Numerical Simulation of Flow and Heat Transfer past a Turbine Blade with a Squealer-Tip," American Society of Mechanical Engineers, Paper 2002-GT-30193, June 2002.

[32]Acharya, S., Yang, H., Ekkad, S. V., Prakash, C., and Bunker, R., "Numerical Simulation of Film Cooling on the Tip of a Gas Turbine Blade," American Society of Mechanical Engineers, Paper 2002-GT-30553, June 2002.

[33]Hohlfeld, E. M., Christophel, J. R., Couch, E. L., and Thole, K. A., "Predictions of Cooling Flow Dirt Purge Holes Along the Tip of a Turbine Blade," 2003-GT-38251, June 2003.

[34]Yang, H., Chen, H. C., Han, J. C., "Numerical Prediction of Film Cooling and Heat Transfer with Different Film Hole Arrangements on the Plane and Squealer Tip of a Gas Turbine Blade," American Society of Mechanical Engineers, Paper 2004-GT-53199, June 2004.

[35]Halila, E. E., Lenahan, D. T., and Thomas, T. T., "Energy Efficient Engine," General Electric Co., NASA CR-167955, June 1982.

[36]Gritsch, M., Schulz, A., and Wittig, S., "Discharge Coefficient Measurements of Film-Cooling Holes with Expanded Exits," American Society of Mechanical Engineers, Paper 97-GT-165, June 1997.

[37]Zhang, L. J., and Jaiswal, R. S., "Turbine Nozzle Endwall Film Cooling Study Using Pressure Sensitive Paint," *Journal of Turbomachinery*, Vol. 123, No. 4, 2001, pp. 730–738.

[38]Wright, L. M., Gao, Z., Varvel, T. A., and Han, J. C., "Assessment of Steady State PSP, TSP and IR Measurement Techniques for Flat Plate Film Cooling," American Society of Mechanical Engineers, Paper HT-2005-72363, July 2005.

[39]Coleman, H. W., and Steele, W. G., *Experimentation and Uncertainty Analysis for Engineers*, Wiley, New York, 1989, pp. 47–131.

[40]Hanjalic, K., "Advanced Turbulence Closure Models, A View of Current Status and Future Prospects," *International Journal of Heat and Fluid Flow*, Vol. 15, No. 3, 1994, pp. 178–200.

[41]Launder, B. E., and Spalding, D. B., "The Numerical Computation of Turbulent Flows," *Computer Methods in Applied Mechanics and Engineering*, Vol. 3, No. 2, 1974, pp. 269–289.

[42]Mhetras, S. P., Yang, H., Gao, Z., and Han, J. C.," Film-Cooling Effectiveness on Squealer Rim Walls and Squealer Cavity Floor of a Gas Turbine Blade Tip Using Pressure Sensitive Paint," GT2005-68387, June 2005.